

1 Article

2 Thermal and electrical characterization of a semi- 3 transparent dye sensitized photovoltaic module 4 under real operating conditions

5 Cristina Cornaro ^{1,2*}, Ludovica Renzi ¹, Marco Pierro ^{1,3}, Aldo Di Carlo ^{2,4} and Alessandro
6 Guglielmotti ⁵

7 ¹ Department of Enterprise Engineering, University of Rome "Tor Vergata" Via del Politecnico,
8 00133 Rome, Italy; cornaro@uniroma2.it; marco.pierro@uniroma2.it; ludovicarenzi@gmail.com.

9 ² CHOSE, , University of Rome "Tor Vergata" Via del Politecnico, 1, 00133 Rome, Italy

10 ³ Institute for Renewable Energy, EURAC Research, 39100 Bolzano, Italy; marco.pierro@eurac.edu

11 ⁴ Department of Electronic Engineering, University of Rome "Tor Vergata" Via del Politecnico,
12 00133 Rome, Italy; aldo.dicarlo@uniroma2.it

13 ⁵ Dyepower, Fonte Nuova, Rome, Italy; alessandro.guglielmotti@gmail.com

14 * Correspondence: cornaro@uniroma2.it; Tel.: +39-06-7259-7233

16 **Abstract:** Dye sensitized solar cell technology is having an important role in renewable energy
17 research due to its features and low cost manufacturing processes. Devices based on this technology
18 appear very well suited for integration into glazing systems due to their characteristics of
19 transparency, color tuning and manufacturing directly on glass substrates. Field data of thermal
20 and electrical characteristics of dye sensitized solar modules (DSM) are important since they can be
21 used as input of building simulation models for the evaluation of their energy saving potential when
22 integrated into buildings. However still few works in the literature provide this information. The
23 study here presented wants to contribute to fill this gap providing a thermal and electrical
24 characterization of a DSM in real operating conditions using a method developed in house. This
25 method uses experimental data coming from test boxes exposed outdoor and dynamic simulation
26 to provide thermal transmittance and solar heat gain coefficient (SHGC) of a DSM prototype. The
27 device exhibits an U-value of 3.6 W/m²K, confirmed by an additional measurement carried on in the
28 lab using a heat flux meter, and a SHGC of 0.2, value compliant with literature results. Electrical
29 characterization evidences an increase of module power with respect to temperature causing DSM
30 suitable for integration in building facades.

31 **Keywords:** DSC; DSM; BIPV; buildings; photovoltaic; thermal properties; electric properties;
32 glazing; energy efficiency

34 1. Introduction

35 New high performing materials for glazing systems have recently received great attention as a
36 mean to improve energy efficiency in buildings. This trend is confirmed by the publication of
37 extensive reviews on the latest developments on glazing technologies in 2015, 2016 and more recently
38 in 2017 [1-4]. Among the emerging systems, photovoltaic semi-transparent materials, (STPV)
39 integrated into windows as active elements, show high potentiality and are starting to be studied
40 more extensively. Characterization of such devices on the point of view of their electrical, optical and
41 thermal behavior in real operating conditions is of fundamental importance to provide reliable data
42 to input into simulation models for the evaluation of their energy saving potential.

43 Chae et al. [5] evaluated the performance of three different amorphous silicon cells when
44 integrated into windows. They built their own cells in the lab and they were able to fully characterize
45 the devices on the optical, thermal and electrical point of view. These data were used as input of an

46 Energy Plus model of a typical office building located in six different climatic zones in US. They
47 concluded that at low and mid latitudes STPV can produce a 30% annual energy saving while for
48 cities like Chicago and Duluth these systems did not provide a real gain. Looking at the
49 Mediterranean area Olivieri et al. performed two studies to characterize energy performance of
50 glazing elements with amorphous silicon for the city of Madrid. They built an experimental set-up to
51 thermally, optically and electrically characterize different kinds of amorphous silicon semi-
52 transparent glasses [6]. They used the experimental data obtained as input of a dynamic building
53 simulation model to evaluate the energy saving potential of STPV elements with different gradation
54 of transparency in Madrid, comparing the results with the energy performance of a standard glazing
55 system [7]. Liao et al. [8] evaluated the energy performance of STPV using amorphous silicon with
56 different characteristics. They demonstrated that a-Si PV glazing hold great potential in terms of
57 energy performance under the climate conditions of Central China.

58 More recently, Wang et al. [9] studied the performance of a PV double skin façade (PV-DSF) and
59 a PV insulating glass (PV-IGU) in a comparative experiment carried on in Hong Kong. The results
60 indicate that the PV-DSF has better performance than PV-IGU in reducing solar heat gains, while it
61 has worse performance regarding thermal insulation. They used the experimental data to validate
62 simulation models to investigate the overall performance of PV-DSF and PV-IGU in five different
63 climates of China. The results show that the average energy saving potential of the PV-DSF and the
64 PV-IGU are 28.4% and 30%, respectively, compared to the commonly used insulating glass window.

65 Organic photovoltaic has a great potential of integration into windows, in particular, Dye
66 Sensitized Solar Modules (DSM) are the most promising devices for this purpose since they are built
67 on glass substrates [10,11]. Recently some works appeared in the literature [12–16] regarding the
68 evaluation of thermal, optical and electrical characteristics of dye sensitized solar technology,
69 however most of them are focused on small dimensions solar cells that usually have better
70 performance than modules. Moreover in laboratory tests the device provides also better performance.
71 These data have been used as input for models to provide energy assessment and potentiality of this
72 technology for energy saving in buildings with different configurations and in different climates. For
73 example Yoon et al. [17] built and characterized their own dye solar cells (DSC) varying the thickness
74 of the active material and used their results as input to a model of an office buildings in Korea
75 provided with DSC windows. They found that lowering transparency of the active material produced
76 low energy consumption in winter mainly due to the PV energy production. This improvement
77 depends on the cell efficiency; at low efficiency levels the energy consumption is almost constant with
78 transparency while if efficiency could double with respect to the actual values a certain dependence
79 of consumption on transparency appeared. Lee et al. [18] evaluated the potential of energy saving of
80 DSC integrated in a reference building in six different climatic zones in the world. They tested six
81 different DSC taking their characteristics from a national database. However the efficiency
82 considered does not seem very representative of the realistic efficiencies of large area devices (DSM)
83 that can be effectively integrated in a glazing system. They evaluated the four DSC performance with
84 respect to four window to wall ratio, four orientations and seven cities. They concluded that while in
85 Berlin and Moscow the advantage is low, a percentage variable between 12% and 22% of energy
86 saving due to PV production is reached for the other cities tested.

87 Recently, Cornaro et al. [19] studied the potential of energy saving of DSM and amorphous
88 silicon modules integrated into a reference building located in different zones in Italy. They
89 evidenced how DSM performs better than thin film even if its use does not provide the necessary
90 saving improvement to reach NZEB conditions for the climatic conditions considered. Reale et al.
91 [20] developed a model of DSM using data coming from outdoor conditions to estimate producible
92 energy of DSM with respect to the well-established technologies for a generic STPV installation. They
93 concluded that DSM should have an equivalent efficiency in real outdoor conditions higher of 16%
94 than the one at standard test conditions in the laboratory (3.36%).

95 Although the recent attempts still few works in the literature regard the evaluation of thermal
96 and electrical properties of DSM for STPV [21], especially in real operating conditions [20,22]. This
97 lack of data can produce not reliable evaluation of DSM potential of energy saving in buildings.

98 The study here presented wants to contribute to fill this gap providing a thermal and electrical
 99 characterization of a DSM in real operating conditions using a method developed in house. In section
 100 2 the method to measure thermal and electrical characteristics of DSM, developed by the authors, is
 101 described. Section 3 presents the results obtained for the thermal characterization, while section 4
 102 shows the results regarding the electrical characteristics of the device.

103 **2. Materials and Methods**

104 Two Solar Test Boxes (STBs) were built with the objective of making comparative analysis of
 105 thermal and lighting performance of transparent material with respect to a double glass reference
 106 pane and to evaluate solar heat gain (SHGC) and U-value of innovative semi-transparent materials.
 107 Here the method is briefly described. More details can be found in Cornaro et al., 2015 [23].
 108



109
110

Figure 1. STB exposed at ESTER lab for the monitoring campaign.

111 The boxes, showed in figure 1, were designed with a linear scale factor of 1:5 and a surface scale
 112 factor of 1:25 with respect to a real room. They have the dimensions of 1.00 m × 0.60 m × 0.55 m and
 113 consist of five opaque walls and one glazed wall. The exterior was manufactured with plywood
 114 panels of 8 mm thickness painted entirely white, to make them highly reflective. The entire not glazed
 115 inner surface of the boxes, also comprising the portion of the area behind the frame of the window,
 116 was heavily insulated with a lightweight rigid insulating material of 80 mm thickness, Stiferite GT,
 117 specific for thermal insulation in buildings. On the south facing wall a glazed area of 42 cm × 37 cm
 118 can be allocated, the remaining of this surface being occupied by a wood frame 90 mm thick, to shield
 119 the thickness of the inside insulating panes.

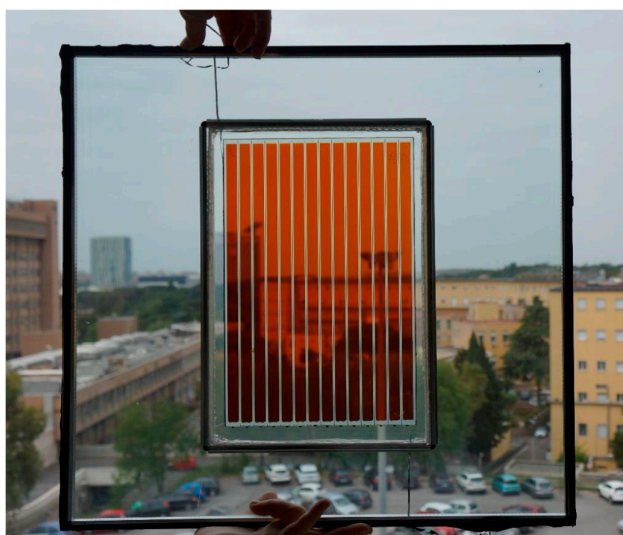
120 **Table 1.** Thermal properties of STB materials.

	Thickness (mm)	Density (kg/m ³)	Specific heat (J/kgK)	Thermal conductivity (W/mK)	Thermal resistance (m ² K/W)	SHGC
Plywood	8	545	1215	0.120	-	-
Insulation	80	36	1453	0.024 (at 10 °C)	3.33	-
Double glazed pane	20	2400	800	1.4	0.34	0.82

121
 122 Each box is instrumented to measure inside air temperature, illuminance and surface
 123 temperature of the inner and outer side of the glazed pane.

124 Temperature sensors are TT500 thermistors by Tecno.el srl with a wide temperature range (-30
 125 to 120 °C), a resolution of 0.1 °C and an accuracy of ± 0.2 °C. Illuminance is measured using a luxmeter
 126 by Delta Ohm srl with a measurement range of 200,000 lx, a sensitivity of 1.5 mV/klx and calibration
 127 accuracy less than 4%. Also outside temperature and relative humidity, solar irradiance on the
 128 vertical plane and wind speed and direction can be measured using a portable weather station.
 129 Temperature and relative humidity are measured by a Rotronic Hygroclip2 sensor with accuracy of
 130 ± 0.1 °C for temperature and of $\pm 0.8\%$ for relative humidity. Solar irradiance sensor is a silicon cell
 131 radiometer provided by Apogee Instruments with an accuracy of $\pm 5\%$ while wind speed and
 132 direction are measured using a model 7911 anemometer provided by Davis Instruments with an
 133 accuracy of ± 1 m/s for speed and of $\pm 7^\circ$ for direction. Data are collected at a minute time rate.
 134 The weather and solar station of ESTER lab (Lat. 41.9, Long. 12.6) [24] provides also direct and
 135 diffuse solar irradiance measurements. Table 1 lists the material properties used in STBs.

136 The experimental activity aimed to evaluate the electrical and thermal performance in real
 137 operating conditions of the DSC module (DSM) shown in figure 2. The active area of the module is
 138 20 cm x 30 cm. In order to fit it into the glass pane of the STB the DSM was inserted into a double
 139 glass pane as shown in the figure.
 140



141
 142 **Figure 2.** The glass system prototype used to test DSM with STB; the red stripes are the dye cells connected to
 143 form the dye sensitized module.

144 The electrical characteristics of DSM are listed in table 2. Current and voltage are evaluated at
 145 nominal conditions, i.e. at Standard Test Conditions (STC). STC are defined as irradiance of 1000
 146 W/m², module temperature of 25°C and irradiance spectrum correspondent to an air mass (AM) equal
 147 to 1.5.

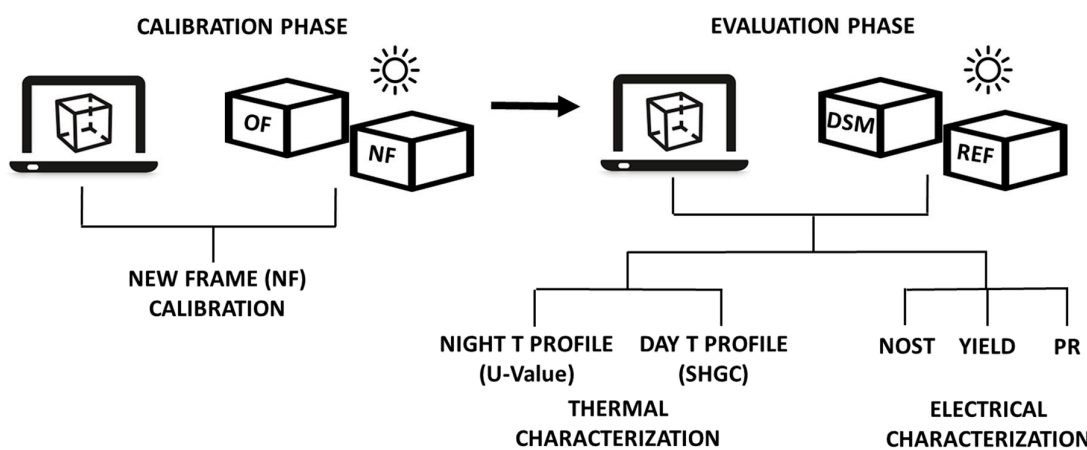
148 **Table 2.** Electrical characteristics of DSM.

Cells area (m ²)	N. of cells	V _{STC} (V)	I _{STC} (mA)
0.011x0.291	14	9.8	150

149
 150 The methodology adopted for this study, schematically shown in the Figure 3 workflow, consists
 151 in the combination of experimental data collection from STB and modeling with a dynamic
 152 simulation software. The process can be divided in two phases, calibration phase and evaluation
 153 phase. The calibration phase is preliminary to the evaluation one. Temperature data collected in one
 154 of the boxes, named "Reference" are used to calibrate the dynamic simulation model of STB. In the
 155 evaluation phase the calibrated model allows to evaluate the thermal transmittance (U) and the solar
 156 heat gain coefficient (SHGC) of the material of unknown characteristics located in the second box,

157 named "Test". In particular, the night temperature profile is used to estimate U, since no contribution
 158 of the solar irradiance to the boxes' thermal loads is present; the daytime temperature profile is used
 159 to evaluate SHGC. The methodology of STB is more deeply described in [23].

160 In particular, since the DSM has to be the only glazed element hit by solar radiation, it was
 161 fundamental providing the two boxes with a suitable wood frame to shield the glazed pane that hold
 162 the DSM. The new frame was bigger than the other used in previous tests of other materials.
 163 Therefore, the calibration phase consisted in the calibration of the new frame (NF) with respect to the
 164 old one (OF) (figure 3). Air temperature data inside STB were collected and used for the calibration
 165 of the dynamic simulation model provided with NF.
 166



167

168 **Figure 3.** Sketch of the method used for the DSM characterization.

169 Each phase is based on the fine-tuning of the air inner temperature's profile measured inside the
 170 boxes with the one simulated by the model. The error is evaluated as the difference between these
 171 two trends: aim of this process is to minimize the error between the two data sets. The index used to
 172 compare experimental and simulated data is the Root Mean Square Error (RMSE), defined as:
 173

$$174 \quad RMSE = \sqrt{\frac{\sum_{i=1}^n (x_i^m - x_i^s)^2}{n}} \quad (1)$$

175

176 where n is the number of data, x_i^m is the i -th measured value, x_i^s is the i -th simulated value.

177 The Normalized Root Mean Square Error is defined as:

178

$$179 \quad NRMSE = \frac{RMSE}{y_{max} - y_{min}} \quad (2)$$

180

181 Where y_{max} and y_{min} are respectively the maximum and the minimum data measured during
 182 the day where RMSE index finds the lowest value.

183 To validate the results obtained for the U-value, an indoor test was also performed and the
 184 results are presented in the next section.

185 During the evaluation phase also the electrical characteristics of the PV glazed pane were
 186 monitored, as shown in figure 1. DSM was connected to a MPPT3000 provided by ISAAC SUPSI,
 187 Lugano. The device allows to keep the module to its maximum power point and to collect IV curves
 188 every 10 minutes during the outdoor campaign. IV curves were used to evaluate the nominal
 189 operative system temperature (NOST), the yield (Y), the efficiency (η) and the performance ratio (PR)
 190 that are defined in section 4.

191 **4. Thermal Characterization**

192 4.1. Calibration phase

193 For the calibration phase a short – term monitoring campaign was carried out from the 12th to
194 the 17th of November 2015. The two boxes, one with the old frame (OF) and the other with the new
195 frame (NF) were exposed outdoor as shown in figure 4. The weather was mostly sunny, with an
196 exception for the 14th of November, when it was mostly cloudy.

197 The boxes were positioned at ESTER lab, with two identical glazed elements (reference double
198 pane) facing south. Meteorological measurements of outside air temperature and relative humidity
199 together with wind speed and direction were also collected using the local station positioned beside
200 the boxes. During the campaign direct and diffuse solar irradiance, useful to run the dynamic
201 simulation, were acquired by a Kypp&Zonen first class CH1 pyrheliometer and a secondary standard
202 CM21 pyranometer, respectively, mounted on a 2AP suntracker available at ESTER lab. Air
203 temperature data inside STB were collected and used for the calibration of the dynamic simulation
204 model provided with NF.

205



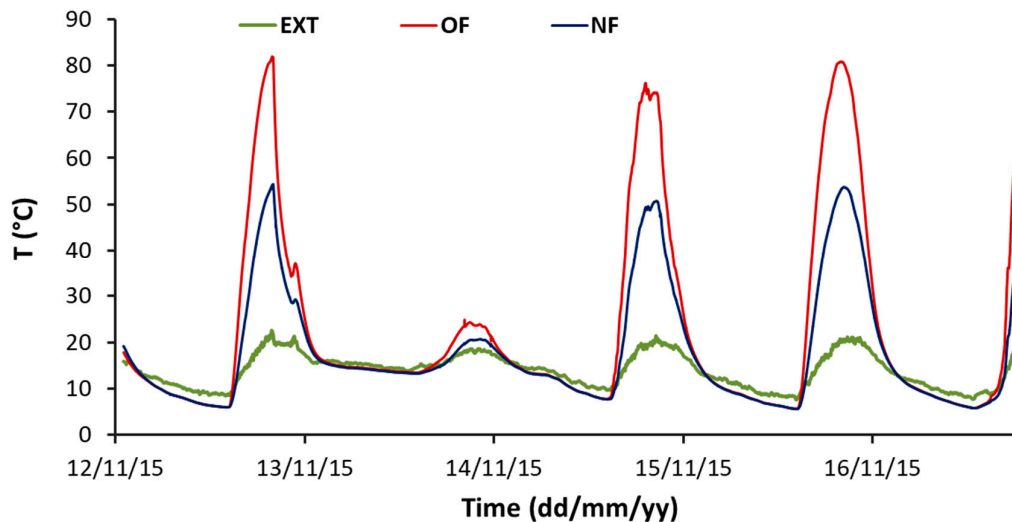
206

207 **Figure 4.** STB test for the new frame calibration.

208 Figure 5 shows the trends of outside and inside air temperature monitored in the two STBs
209 equipped with the reference glazed pane and the two different frames. The inside temperature of
210 both boxes raised up to 50° and more, due to the high insulation properties of the materials and the
211 solar heat gain of the glazing. In particular, the inside temperature of the old framed STB (OF) reached
212 almost 80 °C, or more, while the new framed STB (NF) did not exceed 50 °C. This difference is
213 explained by the reduction of the glazed surface due to the new frame.

214 As a first validation check, the air temperature trend inside the old framed box (OF) was
215 compared with the simulation data provided by the STB original model to verify the old calibration
216 accuracy. A RMSE of 2.72 °C was obtained over the whole period of test with a NRMSE of 4%
217 indicating a good agreement with the original calibration [23].

218 To calibrate the new framed box (NF) the inside air temperature obtained by the STB simulation
219 model was compared with the experimental data; the U-value of the frame and the ratio of opaque
220 over glazed area (frame fraction) were changed in the model till the RMSE reached a minimum. The
221 nighttime period model was used to evaluate the thermal transmittance considering a fixed value of
222 frame fraction. The minimum rate of night RMSE calculated defines the U value which helps
223 minimizing the error, $U = 2 \text{ W/m}^2\text{K}$. The U value was then input in the daytime model so that the air
224 temperature trends simulated varied accordingly to the frame fraction value. The minimum daily
225 RMSE value calculated defined the frame fraction searched to: $F = 0.55$.



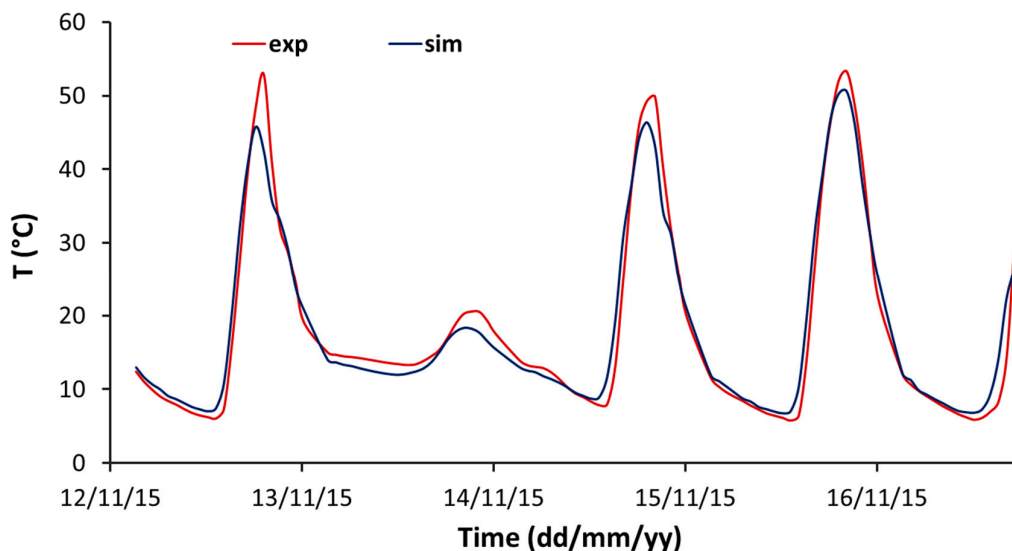
226

227

Figure 5. Temperature trends of ambient air and of the air inside the OF and NF boxes.

228
229

Figure 6 shows the inside air temperature trends of the new framed STB after calibration. A RMSE of 2.56 °C was obtained with a NRMSE of 5.4% over the all period of test.



230

231

Figure 6. Temperature profiles of NF, measured and simulated, after the calibration procedure.

232
233
234

Although the real frame fraction value calculated by the actual geometry of the frame was $F = 0.62$, the best-rated value was 0.55. This difference is probably due to the thermal behavior of the frame-glass sandwich that was taken into account in some way by the model.

235

4.2 Evaluation phase

236
237
238

The evaluation phase was carried out from the 11th to the 21st of April 2016. The boxes were equipped with the new larger frame, one with the reference double glazed pane (REF) and one with the DSM (DSM), as shown in figure 1.

239
240
241
242

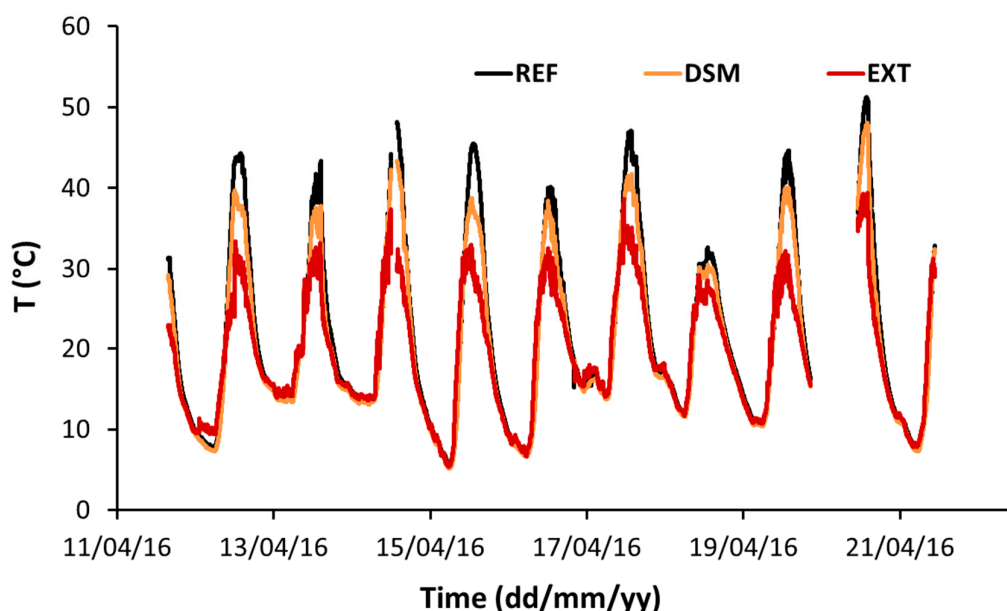
The evaluation phase allowed determining U and SHGC of the DSM sample using data collected during the correspondent monitoring campaign. The U-value was evaluated using the nighttime temperature trend inside the DSM STB while the SHGC was determined using the daytime inside air temperature trend. Weather conditions were mostly variable; the 15th of April was a clear day while

243 the 18th was mostly cloudy. Maximum outside air temperature experienced during the period was
 244 26 °C while the minimum, during the night, was 10 °C, over the whole period. The temperature range
 245 varied between 5 °C and 13°C.

246 The weather data collected during the monitoring campaign were used to produce the climatic
 247 file needed to run the simulation model.

248 Data collected in the REF box where used to validate the calibration carried on in November.
 249 The RMSE and NRMSE evaluated on the whole period of test were equal to 2.79 °C and 6.7%
 250 respectively, confirming the repeatability of the calibration procedure.

251 Fig. 7 shows the inner temperature trends of the REF and DSM boxes, together with the outside
 252 air temperature (EXT). During the monitoring campaign, some data collected got lost, as it can be
 253 seen in the shown trends, due to sensors malfunctioning. The outside air temperature reached almost
 254 26 °C, as already evidenced. As it was expected, the inside temperature of reference glazed pane
 255 raised up to 45 °C while the test box equipped with DSM kept the inside temperature lower.

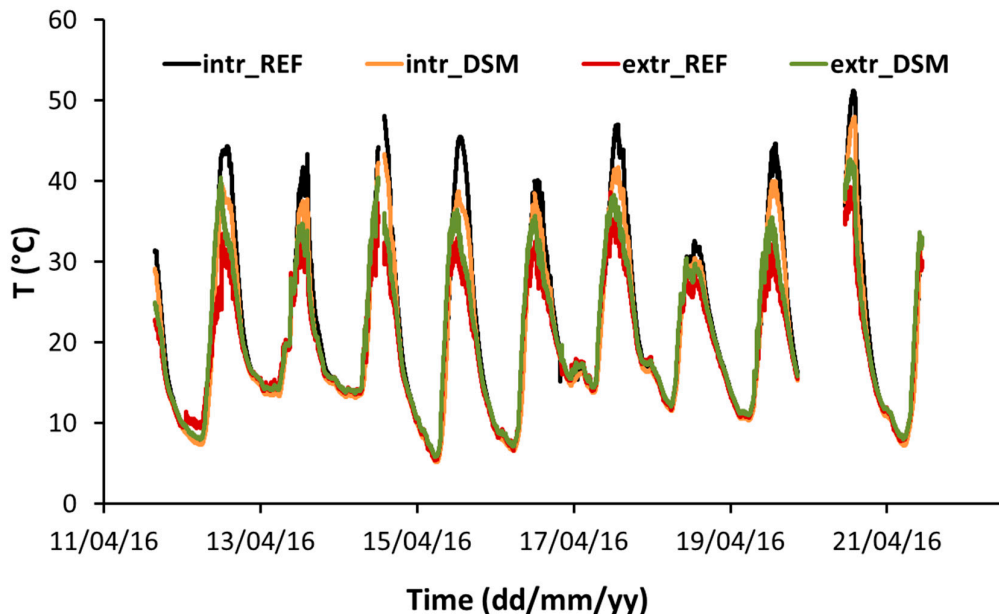


256
 257 **Figure 7.** Temperature trends of air temperature inside REF box and DSM box compared to the
 258 external air temperature.

259 It is interesting to note that during the night inside air temperature of both boxes was lower than
 260 outside air temperature. This is due to radiative heat transfer of the glass pane with respect to the sky
 261 dome. Fig. 8 shows the intrados and extrados surface temperature, for REF and DSM. Both STBs show
 262 intrados temperature higher than extrados, this behavior depends on the heat dynamics between
 263 outdoor and indoor as well as on the thermal properties of the glass [25]. Moreover, extrados
 264 temperature of DSM is higher than REF and this is probably due to different absorption and
 265 transmission coefficients to solar radiation of the two glazed system in the different parts of the solar
 266 spectrum [14].

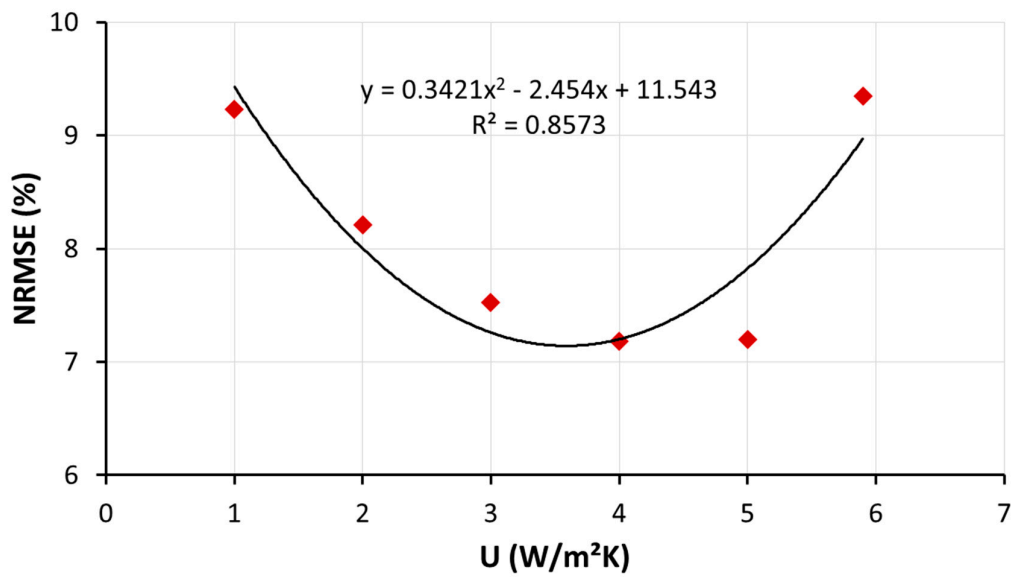
267 The U-value was calculated through a minimization process of the NRMSE between simulated
 268 and calculated night temperature profiles. The calculation of the simulated night temperature profile
 269 used different guessed test sample U-values used as model input. A wide range of possible U-values
 270 was considered, spanning from 1 to 6 W/m²K. A simulation was run for each guess and each
 271 simulated temperature profile obtained was compared to the measured one calculating the NRMSE.

272



273
274 **Figure 8.** Temperature trends of intrados and extrados of REF and DSM box during the period of
275 test.

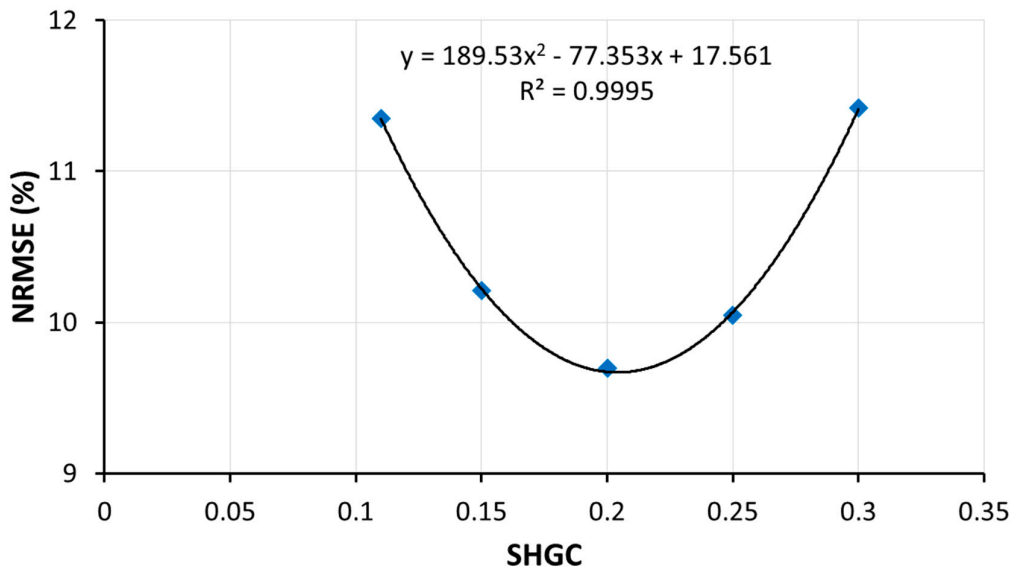
276 Fig. 9 shows the NRMSE values obtained for the various runs, versus U values. As expected, the
277 trend is well approximated by a parabolic trend. The minimum represents the sought value, $U = 3.6$
278 $\text{W/m}^2\text{K}$.



279
280 **Figure 9.** NMRSE versus U-value for the evaluation of U-value of DSM.

281 The U-value obtained is used as input of the daytime model and the SHGC was calculated with
282 the same minimization process used for the U-value. Fig. 10 shows the values obtained for the various
283 runs versus SHGC values. The parabolic trend allows evaluating SHGC = 0.2.

284 It can be observed that for a NRMSE variation of 1% around the minimum a great
285 indetermination of the U and of the SHGC parameters is obtained. The firstly U-value
286 indetermination directly affects the SHGC evaluation.



287 **Figure 10.** NMRSE versus SHGC for the evaluation of SHGC of DSM.

288 This is mainly due to the low sensitivity of the method to the U-value calculation owing to the
 289 small heat flux put into play during the process [23]. For this reason, an additional measurement of
 290 the U-value was carried out with the same box in indoor conditions to validate the result.

291 Moreover, it has to be pointed out that the prototype tested is a combination of simple glass pane
 292 and DSM so that the results could be influenced by the particular configuration considered. However,
 293 this is one of the few characterization of a DSM in real operating conditions and, even if with its
 294 limitations, it can give an indication of the thermal behavior of the system. However the SHGC value
 295 found is in line with what found in the literature for similar devices [21]. Future improvement of the
 296 test will consist in the evaluation of various prototypes with different configurations to investigate
 297 the assembly influence.

298 *4.3 Indoor measurements of U-value*

299 Validation of the U-value outdoor evaluation was carried out using another method in an indoor
 300 environment. The measurement was performed on both boxes, REF and TEST in order to check the
 301 validity of the method and the U-value of the DSM. A heat flux sensor (Albhorn, mod. MA259035)
 302 was applied to REF box which glazed system had known thermal properties (U-value of the glass,
 303 $U_g = 2.8 \text{ W/m}^2\text{K}$) to verify the capability of the method. Two temperature sensors provided by the
 304 heat flux measurement kit were attached to the inside and outside surface of the glass. A laboratory
 305 hotplate with controlled temperature was inserted into the box. In this way a temperature difference
 306 was created between the inside of the box and the outside laboratory. Temperature and heat flux data
 307 were acquired for three hours at a time rate of 30 s, till the steady state was reached. U-value of the
 308 glass was calculated averaging the data referred to the steady state. According to EN673 [26] the U_g
 309 was calculated considering the standard global heat transfer coefficients for inside and outside. Using
 310 this method $U_g = 2.77 \pm 0.03 \text{ W/m}^2\text{K}$ which perfectly fits the results obtained with the outdoor method.
 311 The same procedure was then repeated using the DSM box (figure 11). The U-value obtained for DSM
 312 is $U_{DSM} = 3.68 \pm 0.02 \text{ W/m}^2\text{K}$ confirming what obtained with the outdoor method.

313

314

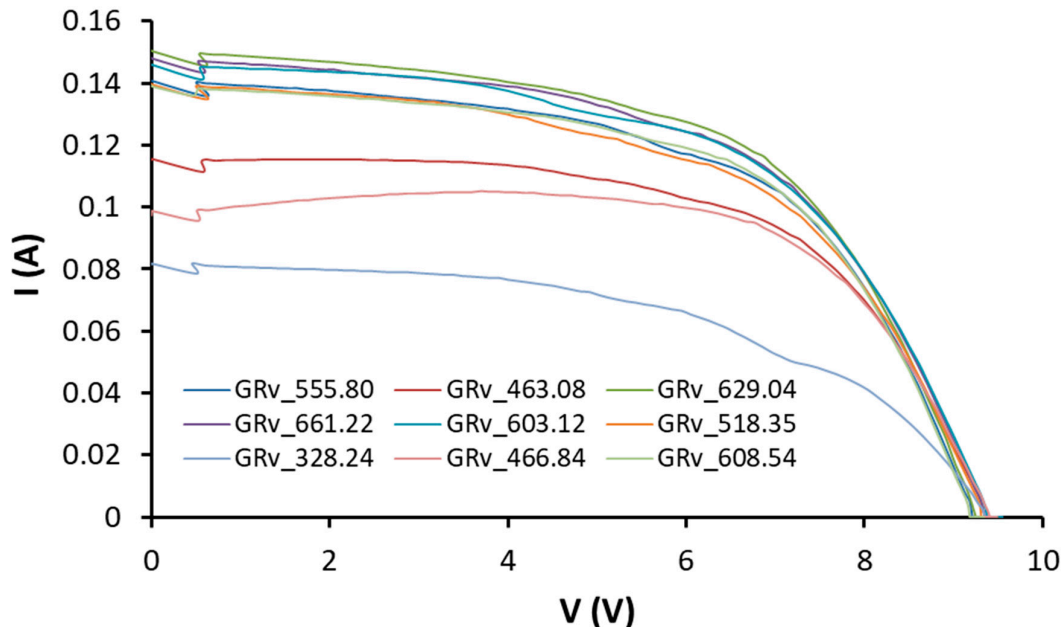


315

316 **Figure 11.** Experimental setup for the laboratory evaluation of U-value of DSM.317 **4. Electrical characterization**

318 According to the electrical specifications provided by the manufacturers, the DSC module
 319 exhibits the nominal characteristics listed in Table 2 with a nominal power declared by the
 320 manufacturer, $P = 1.47$ W. The electrical characterization consisted in the evaluation of the Nominal
 321 Operative System Temperature (NOST), the calculation of the temperature coefficients and the
 322 evaluation of the energy performance during the period of test.

323 The I – V characteristic curve visualizes the operating voltage and electricity values of the
 324 module. Figure 12 shows the I – V curves, one per day, from the 12th of April till the 20th of April,
 325 collected in the central part of the day, when the module experienced its maximum production.



326

327 **Figure 12.** IV curves collected in the central part of each day of test for DSM. GRv is the vertical
 328 global irradiance experienced by DSM.329 *4.1 Performance indices*

330 To evaluate the performance of PV modules of various technologies a series of indices can be
 331 considered. The main index used in the absence of direct measurements on the module is the

332 efficiency at Standard Test Conditions (STC). These conditions are values of irradiance (1,000 W/m²),
 333 module temperature (25 °C) and air mass (AM 1.5) considered as reference for modules properties
 334 evaluation.

335 The efficiency at STC is defined as:

336

$$337 \eta_{STC} = \frac{P_{nom}}{AG_{STC}} \quad (3)$$

338

339 where P_{nom} is the nominal power (or peak power) at STC, A is the surface area of the module and G_{STC}
 340 is the irradiance of 1,000 W/m². This efficiency can be derived from the specification given by the
 341 manufacturer or can be evaluated through indoor measurements using a sun simulator [27].

342 When the PV module is working in the real environment at its maximum power point its real
 343 efficiency can be defined as follow:

344

$$345 \eta = \frac{P_{max}}{AG_{poa}} \quad (4)$$

346

347 where P_{max} is the PV module electrical power produced at the maximum power point of operation
 348 and G_{poa} is the correspondent in plane irradiance. The abovementioned indices evaluate the module
 349 performance instantaneously but they can also give information about the performance in a defined
 350 period of time. In this case instead of electrical power and irradiance the correspondent energy values
 351 in the defined period of time (day, month, year) have to be evaluated. The efficiency indicates the
 352 performance of a device but it does not give indications about its energy production. To evaluate and
 353 to compare the energy production of different modules of different power size, the energy yield is
 354 commonly used. The energy yield (Y) is written as:

355

$$356 Y = \frac{E}{P_{nom}} \quad (5)$$

357

358 where E is the electrical energy produced by the module in a defined time interval and P_{nom} is the
 359 nominal power. This index can also be interpreted as the number of hours in which the PV modules
 360 work at their peak power value. Since the energy production is normalized to the module size, this
 361 index allows comparing PV devices of different peak powers.

362 The energy production of a PV module does not depend only by radiation intensity but also to
 363 some extent to the temperature of the module, to the variation of solar spectrum and also to other
 364 factors that do not strictly depend on the module itself. To take into account all these influences,
 365 another index called Performance Ratio (PR) is defined, [28]:

366

$$367 PR = \frac{Y}{Y_r} ; Y_r = \frac{I}{G_{STC}} \quad (6)$$

368

369 Y_r is called the reference yield and is the ratio between the solar irradiation, I , evaluated in the
 370 considered time interval and the solar irradiance at STC; it also represents the sun peak hours defined
 371 as the hours in which the in plane irradiance has reached 1000 W/m². The PR index can also be seen
 372 as the ratio of the real efficiency over the efficiency at STC, and for this reason it measures how far is
 373 the behaviour of the module with respect to its performance at STC. As already mentioned, this index
 374 is not sensitive to irradiance variation but to secondary effects on the module performance.

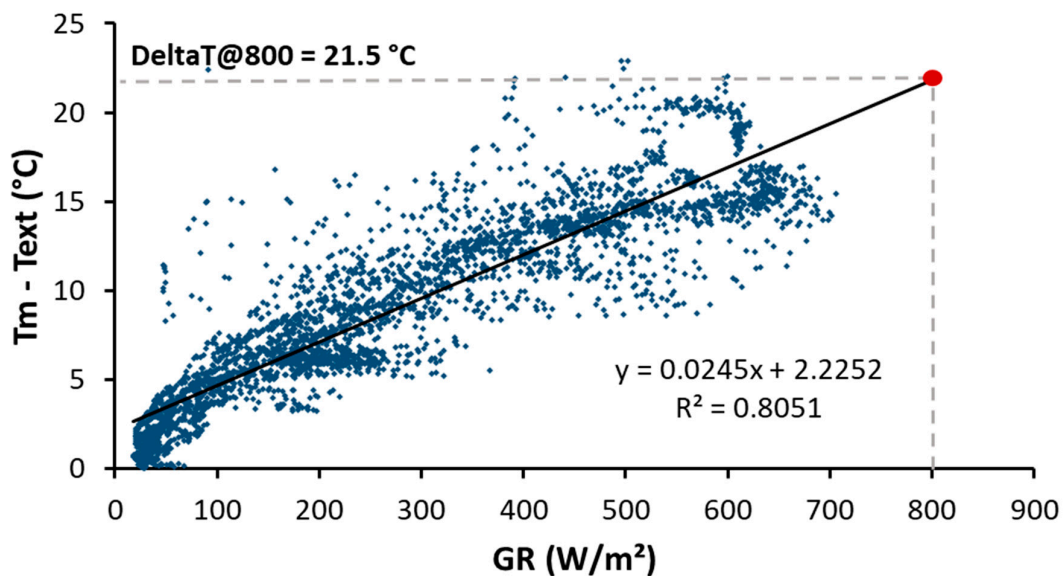
375

4.2 NOST

376

377 Rating the NOST of the module is helpful to foresee future decay of the photovoltaic conversion.
 378 NOST can be seen as the optimal operation temperature of the module. It is defined according to
 379 the Nominal Operating Cell Temperature (NOCT) [29]: NOCT is defined for an open-rack mounted
 module in the following standard reference environment: – tilt angle: 45° from the horizontal – total

380 irradiance: 800 W/m² – ambient temperature: 20°C – wind speed: 1 m/s – no electrical load: open
 381 circuit. NOST differs from NOCT only because it is evaluated when the module circuit is closed on
 382 an electrical load [30]. NOCT and NOST can be used by the system designer as a guide to the
 383 temperature at which a module will operate in the field and it is therefore a useful parameter when
 384 comparing the performance of different module designs. However, these indexes are directly
 385 dependent on the mounting structure, irradiance, wind speed, ambient temperature, reflections and
 386 emissions from the ground and nearby objects, etc. In the present case the same procedure indicated
 387 in [29] was used, however the mounting configuration substantially differs from the one prescribed
 388 in the norm. For this reason the value obtained is not compliant with the norm but can give a good
 389 indication of the operation temperature of the module. The method consists in the measurement of
 390 the temperature difference between the DSM inner surface (T_m) and the outside air temperature.
 391 This value is graphed versus the plane of the module irradiance, as shown in figure 12. A linear
 392 interpolation of the data allows evaluating the temperature difference at the irradiance value of 800
 393 W/m². The NOST value is calculated from this temperature difference considering an outside air
 394 temperature of 20°C. The value obtained is T(NOST) = 41.5 °C. For standard crystalline PV modules
 395 NOCT usually ranges between 40°C and 50°C (typically 45°C). NOST values can be lower than NOCT
 396 [30].



397

398

399 **Figure 13.** Difference between DSM intrados temperature (T_m) and external temperature (Text)
 400 versus solar irradiance for the determination of NOST.

400

4.3 Temperature coefficients

401

402 In a photovoltaic system, peak power is affected by variation of the cell's temperature and of the
 403 global radiation facing the photovoltaic surface. In general, for the most consolidated technologies
 404 when module temperature increases the maximum power decreases. Since temperature has direct
 405 influence of the module performance it is important to know the temperature coefficients of the
 406 considered technology. To evidence the temperature dependence on the DSM performance, power,
 407 P, has been considered at an almost fixed value of vertical global irradiance (GR_v), i.e. $490 \text{ W/m}^2 \leq \text{GR}_v \leq 510 \text{ W/m}^2$.

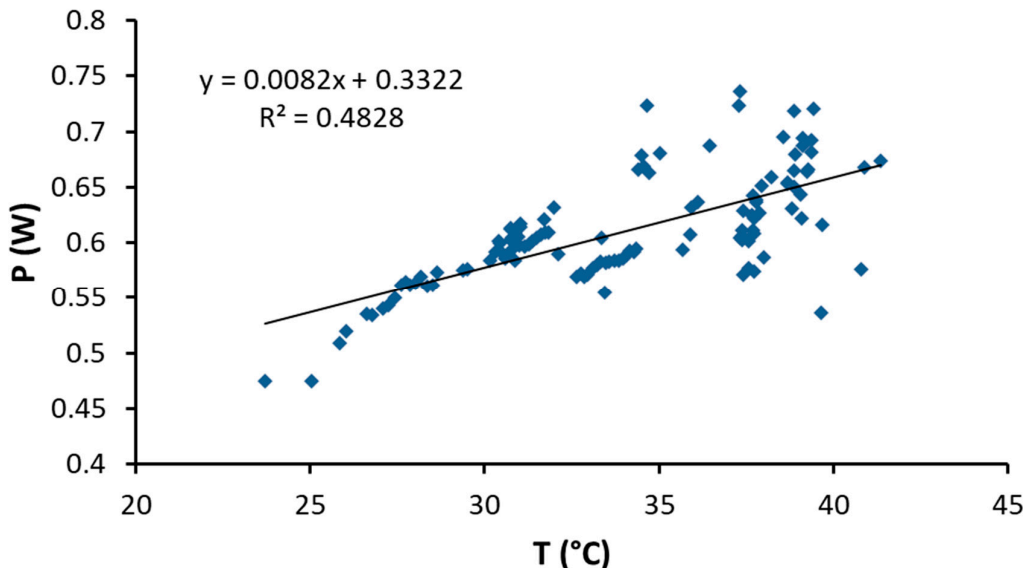
408

409

410

411

412 Figure 14 reports the trend of P, with varying module temperature. The figure shows a positive
 413 trend of the power with increasing temperature showing a positive temperature coefficient of 0.0082
 414 W/°C. This means that PV production increases as temperature increases making DSM suitable for
 415 integration in buildings even if the modules cannot be efficiently cooled.



412
413 **Figure 14.** DSM power versus temperature for the determination of power temperature coefficient.

414 This behavior can be explained considering the total resistance of the cells that is given by the
415 series of conducting glass resistance, RFTO, platinum electrode resistance, RPt and the resistance due
416 to the electron holes carriage in the electrolyte, Rd. It can be observed that as the temperature increases,
417 RFTO remains constant while RPt and Rd increase. In particular it has been observed that for
418 temperature values higher than 40 °C till approximately 50 °C this resistance decrease produces an
419 improvement in the cell efficiency [31]. It has to be noted that the temperature coefficient evaluation
420 was performed with DSM in the vertical position while usually temperature coefficients are
421 measured at normal incidence. In this case the intent was to measure this parameter in more realistic
422 operating conditions. Nevertheless it is possible to compare the result with what obtained for a
423 standard crystalline PV module that is approximately -0.4%/°C. DSM exhibits a power temperature
424 coefficient of 0.6%/°C demonstrating high potentiality for building integration where high
425 temperatures experienced by the PV modules usually penalize standard technologies.

426 **Table 3.** DSM and reference daily yield during the period of test.

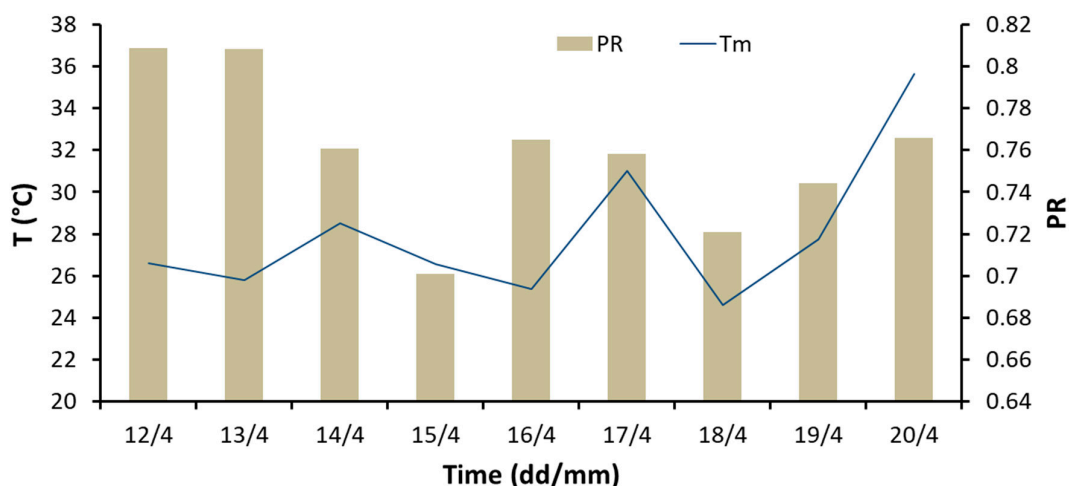
Day	Y (h)	Yr (h)	η (%)
12/04/2016	2.97	3.67	1.80
13/04/2016	2.02	2.50	1.80
14/04/2016	2.23	2.94	1.70
15/04/2016	3.17	4.52	1.56
16/04/2016	2.26	2.96	1.71
17/04/2016	3.03	3.99	1.69
18/04/2016	1.52	2.11	1.61
19/04/2016	2.87	3.86	1.66
20/04/2016	2.04	2.66	1.71

427 *4.3 Energy performance*

428 Figure 14 reports the average daily values of PR has defined in section 4.1. Table 3 summarizes
429 the daily reference and DSM yield together with the DSM daily efficiency.
430 The overall energy produced by the module operating during the monitoring campaign is 32.05 Wh.
431 The average PR for the total time period considered is 0.76. Average efficiency over the period of test

432 is 1.69 %, to be compared with $\eta_{STC} = 3.28\%$. Figure 14 reports the daily PR together with the average
 433 diurnal temperature of the back of the module. It appears difficult to explain the daily PR trend since
 434 the index is fluctuating day by day. For example, it is not clear why on the 15th of April, the day with
 435 the highest solar irradiance, DSM gave such a low performance and efficiency (see also table 3). This
 436 behavior does not seem to be related to temperature variations (see figure 14) but rather to
 437 instabilities of the module. At present it is not possible to give a clear explanation of the results.
 438 Further investigations are necessary to deepen this topic.

439
 440



441
 442 **Figure 15.** Daily PR, and diurnal average module temperature of DSM during the days of test.
 443

444

4. Conclusions

445 In the work here presented a complete characterization of a dye sensitized PV module, suitable
 446 for building integration, was carried on in real operating conditions. A methodology developed by
 447 the authors, using solar test boxes, allowed evaluating the U-value and the SHGC of a DSM prototype
 448 in outdoor conditions. During the same test also the electrical characteristics of the module were
 449 measured and the energy production, the efficiency and performance ratio were determined. The
 450 thermal characterization provided a U-value = 3.6 W/m²K and a SHGC = 0.2. U-value was validated
 451 through a steady state indoor test while SHGC results compliant with data found in the literature.
 452 Electrical characterization evidenced a favorable performance of the module with respect to
 453 increasing temperatures. This behavior proves that DSM could be integrated into building facades
 454 with success. No clear explanation could be given for the daily energy production trend of DSM and
 455 its daily energy performance. Future investigations are needed to deepen this aspect. These results
 456 can be helpful for a more realistic evaluation of energy saving potential of dye sensitized solar cell
 457 technology integrated into buildings since they can be used as realistic input for building dynamic
 458 simulation models.

459 **Author Contributions:** Cristina Cornaro conceived and designed the experiments; Ludovica Renzi performed
 460 the experiments; Ludovica Renzi, Marco Pierro and Cristina Cornaro analyzed the data; Alessandro
 461 Guglielmotti and Aldo di Carlo built and contributed dye sensitized module and its specifications; Cristina
 462 Cornaro wrote the paper.

463 **Conflicts of Interest:** The authors declare no conflict of interest.

464 References

465 1. Cuce, E.; Riffat, S. B. A state-of-the-art review on innovative glazing technologies. *Renew. Sustain. Energy Rev.*
 466 2015, 41, 695–714.

467 2. Saifullah, M.; Gwak, J.; Yun, J. H. Comprehensive review on material requirements, present status, and future
468 prospects for building-integrated semitransparent photovoltaics (BISTPV). *J. Mater. Chem. A* **2016**, *4*, 8512–8540.

469 3. Skandalos, N.; Karamanis, D. PV glazing technologies. *Renew. Sustain. Energy Rev.* **2015**, *49*, 306–322.

470 4. Rezaei, S. D.; Shannigrahi, S.; Ramakrishna, S. A review of conventional, advanced, and smart glazing
471 technologies and materials for improving indoor environment. *Sol. Energy Mater. Sol. Cells* **2017**, *159*, 26–51.

472 5. Chae, Y. T.; Kim, J.; Park, H.; Shin, B. Building energy performance evaluation of building integrated
473 photovoltaic (BIPV) window with semi-transparent solar cells. *Appl. Energy* **2014**, *129*, 217–227.

474 6. Olivieri, L.; Caamaño-Martin, E.; Olivieri, F.; Neila, J. Integral energy performance characterization of semi-
475 transparent photovoltaic elements for building integration under real operation conditions. *Energy Build.* **2014**,
476 *68*, 280–291.

477 7. Olivieri, L.; Caamaño-Martín, E.; Moralejo-Vázquez, F. J.; Martín-Chivelet, N.; Olivieri, F.; Neila-Gonzalez, F.
478 J. Energy saving potential of semi-transparent photovoltaic elements for building integration. *Energy* **2014**, *76*,
479 572–583.

480 8. Liao, W.; Xu, S. Energy performance comparison among see-through amorphous-silicon PV (photovoltaic)
481 glazings and traditional glazings under different architectural conditions in China. *Energy* **2015**, *83*, 267–275.

482 9. Wang, M.; Peng, J.; Li, N.; Yang, H.; Wang, C.; Li, X.; Lu, T. Comparison of energy performance between PV
483 double skin facades and PV insulating glass units. *Appl. Energy* **2017**, *194*, 148–160.

484 10. Fakharuddin, A.; Jose, R.; Brown, T. M.; Fabregat-Santiago, F.; Bisquert, J. A perspective on the production
485 of dye-sensitized solar modules. *Energy Environ. Sci.* **2014**, *7*, 3952–3981.

486 11. Cornaro, C.; Carlo, A. Di Organic Photovoltaics and Energy Efficiency in Buildings. In *Nano and Biotech based*
487 *material for energy building efficiency*; Torgal, Pacheco, Buratti, Cinzia, Kalaiselvam, Siva, Granqvist, Claes-Göran,
488 Ivanov, V., Ed.; Elsevier Ltd, 2016; pp. 321–355.

489 12. D'Ercole, D.; Dominici, L.; Brown, T. M.; Michelotti, F.; Reale, A.; Di Carlo, A. Angular response of dye solar
490 cells to solar and spectrally resolved light. *Appl. Phys. Lett.* **2011**, *99*, 1–4.

491 13. Tian, H.; Yu, X.; Zhang, J.; Duan, W.; Tian, F.; Yu, T. The influence of environmental factors on DSSCs for
492 BIPV. *Int. J. Electrochem. Sci.* **2012**, *7*, 4686–4691.

493 14. Kang, J. G.; Kim, J. H.; Kim, J. T. Performance evaluation of DSC windows for buildings. *Int. J. Photoenergy*
494 **2013**, *2013*.

495 15. Kang, J. G.; Kim, J. H.; Jang, H. Bin; Kim, J. T. Characteristics of DSSC panels with silicone encapsulant. *Int.*
496 *J. Photoenergy* **2015**, *2015*.

497 16. Mastroianni, S.; Lanuti, A.; Penna, S.; Reale, A.; Brown, T. M.; Di Carlo, A.; Decker, F. Physical and
498 electrochemical analysis of an indoor-outdoor ageing test of large-area dye solar cell devices. *ChemPhysChem*
499 **2012**, *13*, 2925–2936.

500 17. Yoon, S.; Tak, S.; Kim, J.; Jun, Y.; Kang, K.; Park, J. Application of transparent dye-sensitized solar cells to
501 building integrated photovoltaic systems. *Build. Environ.* **2011**, *46*, 1899–1904.

502 18. Lee, J. W.; Park, J.; Jung, H. J. A feasibility study on a building's window system based on dye-sensitized
503 solar cells. *Energy Build.* **2014**, *81*, 38–47.

504 19. Cornaro, C.; Basciano, G.; Puggioni, V.; Pierro, M. Energy Saving Assessment of Semi-Transparent
505 Photovoltaic Modules Integrated into NZEB. *Buildings* **2017**, *7*, 9.

506 20. Reale, A.; Cinà, L.; Malatesta, A.; De Marco, R.; Brown, T. M.; Di Carlo, A. Estimation of Energy Production
507 of Dye-Sensitized Solar Cell Modules for Building-Integrated Photovoltaic Applications. *Energy Technol.* **2014**, *2*,
508 531–541.

509 21. Bouvard, O.; Vanzo, S.; Schüller, A. Experimental determination of optical and thermal properties of semi-

510 transparent photovoltaic modules based on dye-sensitized solar cells. *Energy Procedia* **2015**, *78*, 453–458.

511 22. Cornaro, C.; Bartocci, S.; Musella, D.; Strati, C.; Lanuti, A.; Mastroianni, S.; Penna, S.; Guidobaldi, A.;

512 Giordano, F.; Petrolati, E.; Brown, T. M.; Reale, A.; Di Carlo, A. Comparative analysis of the outdoor performance

513 of a dye solar cell mini-panel for building integrated photovoltaics applications. *Prog. Photovoltaics Res. Appl.*

514 **2015**.

515 23. Cornaro, C.; Bucci, F.; Pierro, M.; Bonadonna, M. E.; Siniscalco, G. A new method for the thermal

516 characterization of transparent and semi-transparent materials using outdoor measurements and dynamic

517 simulation. *Energy Build.* **2015**, *104*, 57–64.

518 24. Spena, A.; Cornaro, C.; Serafini, S. Outdoor ESTER test facility for advanced technologies PV modules. In

519 *Conference Record of the IEEE Photovoltaic Specialists Conference*; 2008.

520 25. Wang, T. P.; Wang, L. B. A steady heat transfer model of hollow double glazing under entire wave length

521 heat radiation. *Energy Build.* **2014**, *81*, 72–83.

522 26. EN673 Glass in building. Determination of thermal transmittance (U value). Calculation method 2011.

523 27. IEC 60904-2. “Photovoltaic devices –Part 2: Requirements for reference solar devices”. 2007.

524 28. Marion, B. Performance Parameters for Grid-Connected PV systems. In *Proceedings of the 31st IEEE*

525 *Photovoltaics Specialists Conference*; Lake Buena Vista, Florida, January 3-7, 2005., 2005.

526 29. IEC 61215. Crystalline silicon terrestrial photovoltaic (PV) modules Design qualification and type approval

527 2005.

528 30. M. Pellegrino, C. Cornaro, S. Bartocci, G D'Angiolini, G. Flaminio, V. Giglio, A. Matano, G. Nardelli, A.;

529 Spena, O. and A. Outdoor measurements for an effective PV modules temperature characterization. In

530 *Proceedings of the 24th EUPVSEC Conference*; 2009; pp. 2–6.

531 31. Raga, S. R.; Fabregat-Santiago, F. Temperature effects in dye-sensitized solar cells. *Phys. Chem. Chem. Phys.*

532 **2013**, *15*, 2328.

533